Soft Matter

Dynamic Article Links ►

Cite this: DOI: 10.1039/c0xx00000x

www.rsc.org/xxxxxx

ARTICLE TYPE

Capillary Micromechanics for Core-Shell Particles

Tiantian Kong [a,b], Liqiu Wang [a,b]*, Hans M. Wyss [c]*, and Ho Cheung Shum [a,d]*

Received (in XXX, XXX) Xth XXXXXXXXX 20XX, Accepted Xth XXXXXXXXX 20XX
DOI: 10.1039/b000000x

In this work, we have developed a facile, economical microfluidic approach as well as a simple model description to measure and predict the mechanical properties of composite core-shell microparticles made from materials with dramatically different elastic properties. By forcing the particles through a tapered capillary and analyzing their deformation, the shear and compressive moduli can be measured in one single experiment. We have also formulated theoretical models that accurately capture the moduli of the microparticles in both the elastic and the non-linear deformation regimes. Our results show how the moduli of these core-shell structures depend on the material composition of the core-shell microparticles, as well as on their microstructures. The proposed technique and the understanding enabled by it also provide valuable insights into the mechanical behavior of analogous biomaterials, such as liposomes and cells.

1. Introduction

Soft and deformable composite microparticles are common in biological systems and industrial products such as cosmetics, pharmaceuticals, foods and functional textiles [1–7]. Such microparticles with core-shell structures are especially important for applications such as encapsulation and controlled release, contrast enhancement in ultrasonic imaging and photonics[8–14,4,2,3]. In these applications, the mechanical properties of core-shell microcapsules are of key importance. Mechanical properties control the conditions under which the core-shell microcapsules are deformed elastically, plastically or even ruptured[15–24]. They directly determine the volumetric and shape changes of the microcapsules under an applied external stress[25,26], which for soft and biological materials can be surprisingly large. For instance, biological microcapsules such as red blood cells can pass through capillary vessels that are much smaller than their equilibrium diameters, thereby circumventing the clogging of the blood vessels[27–29,16]. Mechanical properties are also critical in the design of structures such as core-shell microcapsules, for instance, used as controlled microenvironments for the growth and regeneration of cells[30] and tissues.

Knowledge about the mechanical response of microcapsules thus allows us to predict and design their behavior, especially in constricted geometries, such as blood vessels or porous media. For drug delivery applications, it is also important to precisely measure the mechanical properties of core-shell microcapsules. Unfavorable mechanical properties can be a serious limitation to the performance of these materials in practical applications. For instance, a shell that should stabilize and contain the core materials may rupture prematurely, prior to the desired delivery at the target site. Conversely, a core-shell capsule that is mechanically too stiff cannot squeeze through small blood vessels, thus potentially causing embolism[31–33]. The ability to design core-shell microcapsules with precisely controlled mechanical properties, and the availability of experimental methods for directly measuring these properties are thus of critical importance.

However, the measurement of mechanical properties at the microscopic scale is not straightforward[34–36]. Atomic Force Microscope (AFM) or Micropipette Aspiration are methods that are often employed for measuring single cell mechanics[37,38]; they can also be used to characterize the mechanical properties of isotropic soft particles at the microscopic scale[39–41,38]. With AFM, a force extension curve is obtained by indenting a single particle with an AFM tip. For isotropic elastic objects, such measurements yield information on the Young's modulus of the material, but this requires an assumption to be made about the Poisson ratio of the material[37,40]. Moreover, as the indentation of the AFM tip is highly localized near the top surface of the object, in the case of an anisotropic structure, the measured response may not represent the behavior of the entire object. Micropipette Aspiration measures the elastic properties of single biological cells and membranes by applying a negative pressure, thereby partly sucking them into a capillary[39,38,41]. The degree to which the cells are deformed in response to such an applied negative pressure is a measure of its elastic properties. This technique allows characterization of cells through contact between a part of the membrane and the pipette wall; however, the overall response of the entire soft object is not easily obtained. Results also depend sensitively on the surface or membrane properties.

Recently proposed methods circumvent this problem by deforming the entire soft objects, such as cells and droplets, in microchannels to correlate their elasticity to velocity, and use this correlation for sorting cells/droplets/particles[42–46]. Quantitative measurement of the full elastic properties, given by both the shear and compressive elastic moduli is enabled by a recently developed Capillary Micromechanics technique [26,25]. Capillary

micromechanics allows accurate measurement of both the shear and compressive elastic moduli of homogeneous soft particles by quantifying their average deformation [26,25]; the method has been previously validated by comparing the measured values with those obtained with conventional, well-established methods such as macroscopic compression measurements,[25] osmotic compression, [26] and atomic force microscopy [47]. Since the method is straightforward and can readily be integrated into microfluidic devices, it is an ideal tool for measuring mechanical properties at the single particle level.

However, thus far, this approach has only been applied to studies of homogenous soft particles. Inhomogeneous soft objects, such as core-shell particles, which represent an important structure for biology and biomedical applications, remain difficult to characterize. The overall properties of such particles will depend on the bulk properties of both the shell and the core material, as well as the internal structure of the particles. To control and understand the mechanics of these systems, it is thus essential to investigate and understand the relationship between the respective properties of core and shell, their microstructures and their effects on the overall mechanical properties of the microparticles. Based on such understanding, design principles can be established allowing us to precisely tailor the mechanical behavior of composite microparticles to a desired application.

In this paper, we probe the mechanical properties of core-shell microparticles in which cores and shells are made from drastically different materials. We investigate the relationship between the mechanical properties of these core-shell microparticles and their material composition, as well as their microstructures. By the development and validation of a simple model, the prediction and design of soft composite microparticles with mechanical properties that are specifically tailored to the desired applications are enabled. This applies in particular to applications where the soft particles undergo a mode of deformation similar to that probed in our experiments, where particles are squeezed in circular tube geometry; this is exactly the mode of deformation that is experienced by cells and soft objects in the blood stream, as they pass through small blood vessels. An improved understanding of the relationship between the composition, structure, and the mechanical properties of microparticles could thus also provide valuable insight into the performance and behavior of core-shell particles made for drug-delivery applications, or of analogous biomaterials with core-shell morphologies similar to those of liposomes and cells.

2. Experimental

2.1 Capillary Micromechanics setup

To characterize the mechanical properties of the core-shell microparticles, we use a glass microfluidic device, based on a tapered glass capillary, as shown in Figure 1. Initially, we apply a small pressure difference that causes the microparticles to flow towards the tip, until the first particle arrives in the tapered tip section of the capillary and clogs the capillary, thereby blocking the further flow of fluid. At this point the entire applied pressure difference will fall off across the microparticle blocking the flow. In the absence of fluid flow, this pressure difference is balanced by the internal elastic stresses that occur as a result of the particle deformation. In equilibrium, the microparticle is no longer moving and the externally applied stress must be fully balanced by this internal elastic stress. In the absence of static friction between the particle and the capillary wall, the external forces acting on the particle can be derived based on the applied pressure difference and the tapering angle [25,26] (see details of the derivation in supplementary information). The effect of friction is neglected for hydrogel materials since they exhibit very low friction coefficients with a glass surface [48,25,26]. Thus, by quantifying the particle deformation as a result of the applied pressure difference, the elastic properties of a single microparticle can be measured. The deformation process of the core-shell microparticle corresponding to each pressure difference is recorded by an optical microscope (Motic 2000), equipped with a digital camera (MotionPro X4). We analyze these microscopic images using the open source software *ImageJ*, and calculate the corresponding particle deformations and geometries using a MATLAB script.

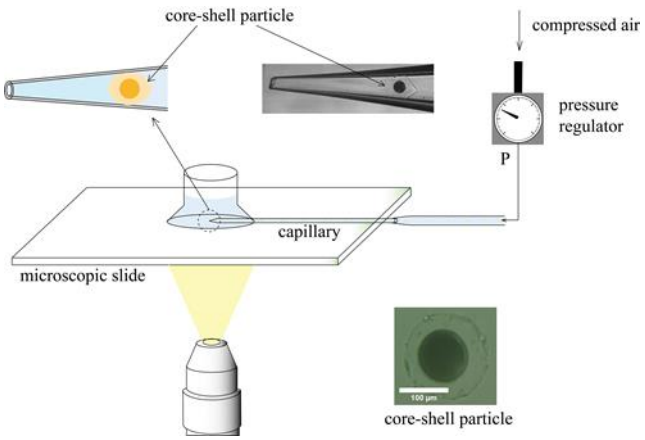

Fig. 1 Schematic of experimental set-up; (inset) microscopic image of a typical microparticle used.

2.2 Fabrication of single and core-shell microparticles

In our experiment, we choose a core material that is relatively rigid and extensively used in controlled release studies, poly(lactic-co-glycolic acid) (PLGA). For the shell material we use the natural polymer alginate, which is also commonly used in a wide range of biomedical applications.

To prepare core-shell microparticles, we use oil-in-water-in-oil (O/W/O) double emulsions as templates. To create particles with uniform sizes and geometries, capillary microfluidics is used to generate monodisperse O/W/O double emulsion, as shown in Figure 2 (A-C). We use 0.04 gml^{-1} poly(lactic-co-glycolic acid) (PLGA) in dichloromethane as core phase, 1 wt% alginate with 1 wt% polyvinyl alcohol (PVA) in DI water for the shell phase, and toluene with 10 wt% span 80 for the continuous phase. Both PVA and span 80 are surfactants used to stabilize the double emulsions. In order to form solid-like core-shell structures from these emulsion templates, the emulsions produced in the microfluidic device are injected into a mixture of calcium chloride and ethanol, which leads to solidification of both the core and the shell material: The calcium ions react with alginate in the shell phase to form solid shells, ethanol is added to accelerate the solidification process as it is miscible with both toluene and water; finally, rigid PLGA cores are formed as dichloromethane evaporates. Thus the double emulsion droplets

are solidified into core-shell microparticles, where a rigid PLGA core is surrounded by a soft alginate shell. The core-to-shell ratio can easily be tuned by adjusting the flow rate of the three inlet phases in the microfluidic flow focusing device. We keep the flow rate for the shell and continuous phase fluids constant at 450 μL $h^{-1}$and 3500 μL h^{-1}; by flowing the core fluid at 100 μL h^{-1}, 200 μL h^{-1}, and 400 μL h^{-1}, we obtain core-shell size ratios of 0.65, 0.5, and 0.4, respectively, as shown in Figure 2 (D-G). As expected, the core-to-shell ratio scales approximately as the cube root of the ratio between the expected core volume and particle volume, $d_{core}/d_{shell} \sim [Q_{core}/(Q_{core}+Q_{shell})]^{1/3}$, as indicated by the linear fit with an exponent n=1 to the data shown in Figure 2 (H).

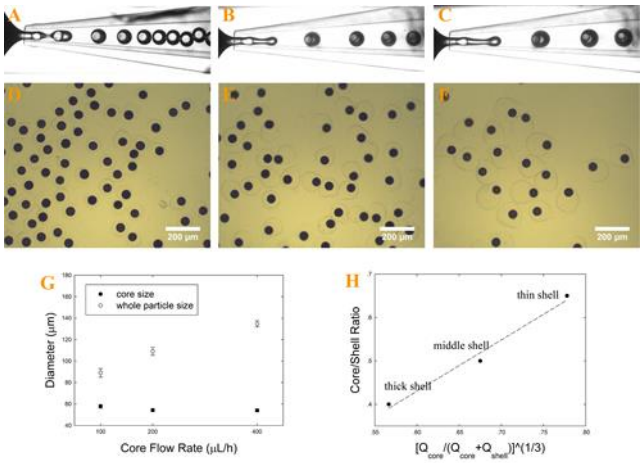

Fig.2 Microfluidic generation of double emulsion template droplets. Core, shell and continuous phases are 0.04 gml^{-1} PLGA in dichloromethane, 1 wt% alginate with 1 wt% PVA, and toluene with 10% Span-80 surfactant respectively. The core phase flow rates in (A), (B), (C) are 400 μL h^{-1}, 200 μL h^{-1}, 100 μL h^{-1} respectively. The flow rates of the shell and continuous phase are kept at 450 μL $h^{-1}$and 3500 μL $h^{-1}$for (A-C). (D-F) Optical microscope images of solidified core-shell microparticles of different shell thickness, with the cores and shells being PLGA and alginate respectively; G) Averages and standard deviations of the measured diameters of the core and the overall particle. H) Core-to-shell ratios of the microparticles obtained at the three different applied flow conditions. The dashed line shows a power-law fit to the data, with an exponent of 1.

3. Results and discussions

To study the mechanical response of these core-shell structures, we use the Capillary Micromechanics technique, as shown schematically in Figure 3 (A-C). The typical shear and compressive stress response of core-shell microparticles with core-to-shell ratio 0.5 is shown in Figure 3 (D-E). In both shear and compression, the characteristic stress increases linearly with the applied characteristic strain deformation when the strain deformation is small. Moreover, the linear elastic properties of PLGA-alginate microparticles lie between those of single component PLGA and alginate microparticles, the elastic properties of which are also acquired using capillary micromechanics (Figure S1 (A-B)). However, we also observe a nonlinear elastic response of the core-shell particles above a critical deformation, where the stress no longer depends linearly on the applied strain. Instead, a strain stiffening behavior where both moduli increase with increasing deformation is observed, as shown in Figure 3 (D-E). We expect the core-to-shell ratio of the microparticles to play an important role in determining both the linear elastic response, as well as the onset and extent of this non-linear strain stiffening behavior.

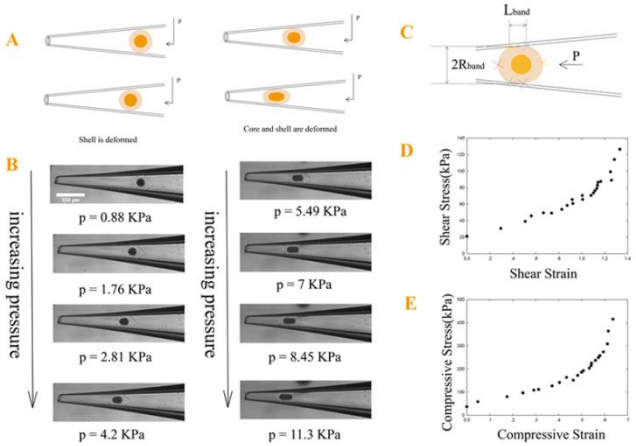

Fig.3 Capillary micromechanics A) schematic B) measurement for PLGA-alginate core-shell microparticle; the particle deforms and moves towards the tip of the tapered capillary as the applied pressures increases. C) Schematic representation of the geometrical characteristics in image analysis. L_{band} is the length of the contact area between the particle and capillary wall, R_{band} is the average radius of the particle from the center to the contact area. Typical results from Capillary Micromechanics measurement for PLGA-alginate core-shell microparticles: the shear D) and E) compressive modulus is analyzed by plotting the stress as a function of characteristic strain.

To study the influence of the core-to-shell ratio on the linear elastic properties, we vary the core-to-shell size ratios α and measure the corresponding shear and compressive responses. Indeed, the response of core-shell particles depends systematically on α ((Figure 4 (A-B)). The overall shear and compressive moduli of the core-shell microcapsules increase systematically as the core-to-shell ratio is increased.

To estimate the influence of the core-to-shell ratio on the overall elastic moduli of the particles, we apply a Maxwell rule of mixtures by assuming that the shear and compressive moduli, K and G, of composite core-shell microcapsules can be expressed as a sum of the respective moduli of the two components weighted by their volume ratios:

$$K_{composite} = \alpha^3 K_{core} + (1-\alpha^3) K_{shell} \text{ , and} \quad \text{Eq. (1).}$$

$$G_{composite} = \alpha^3 G_{core} + (1-\alpha^3) G_{shell} \text{ .} \quad \text{Eq. (2).}$$

This simple estimation is in surprisingly good agreement with our experimental results, as shown in Figure 4 (C), where data for the pure core and the pure shell particles correspond to α=1 and α=0, respectively. A change in α leads to a systematic variation of the mechanical properties, in agreement with the simple predictions of Eq. (1-2). In principle, by varying the core-to-shell ratio of the particles, the modulus of the particles can be tuned to any value that lies in between those of the core and the shell materials. These results thus offer a simple guideline for precisely controlling the linear elastic properties of core-shell composite microparticles.

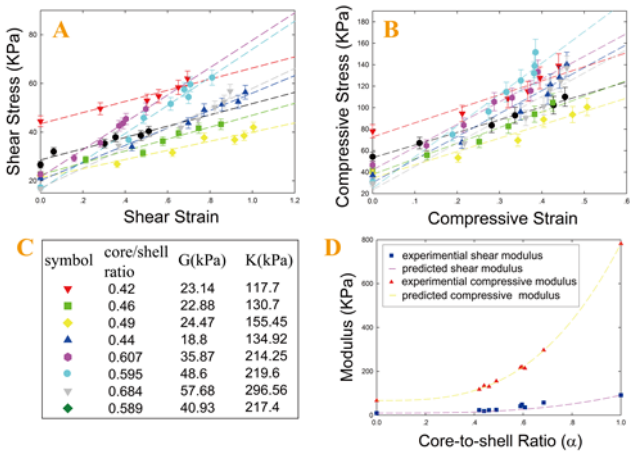

symbol	core/shell ratio	G(kPa)	K(kPa)
▼	0.42	23.14	117.7
■	0.46	22.88	130.7
◆	0.49	24.47	155.45
▲	0.44	18.8	134.92
●	0.607	35.87	214.25
●	0.595	48.6	219.6
▼	0.684	57.68	296.56
◆	0.589	40.93	217.4

Fig.4 Linear elastic behavior of core-shell particles: A) Shear and B) compressive modulus analysis for PLGA-alginate core-shell microparticles in the linear deformation range, where the stress depends linearly on the strain deformation. C) The shear and compressive modulus of core-shell particles with different core-to-shell rations in linear deformation range D) Elastic compressive (triangles) and shear modulus (squares) of core-shell microparticles as a function of the core-to-shell ratio α. The behavior is well predicted by a volume weighted average of the core-shell material properties, shown as dashed lines. The experimental error, indicated as error bars, is estimated based on an error propagation analysis[25]; main sources of error are the accuracy of the applied pressure difference and the spatial precision in digital image analysis.

To further investigate the elastic properties of these core-shell particles, we extend our analysis to larger deformations, where the particles exhibit strain stiffening. To rationalize this strain stiffening behavior, we approximate the shape of the core-shell microparticle and of its core as two cylinders with circular cross-section inside the circular capillary, as shown in Figure 5 (A). As the applied pressure increases, the core-shell particle moves towards the tip of the tapered capillary. This corresponds to an elongation of the cylinders upon compression by the capillary wall (Figure 5 (A)). Since the radius of the microparticle is small, and the taper angle of the capillary is also small, for simplicity we approximate the shape of the particle and the core as straight circular cylinders. As a result of this approximation of shape, the small tapering angle is neglected since it only affects the resulting stress and strain within the particle by a factor of ~ $\mathbf{1/\sin\alpha}$, with the real stresses expected to be larger near the tip and lower near the rear of the particle. Instead of taking these small variations into account, here we set a constant stress along the length of the particle by assuming a cylindrical shape of the deformed particle. The core-shell particle then consists of three main sections, the middle section where the core is present and two single-component sections at the front and back ends of particle, as shown in Figure 5 (B). To estimate the effective stress response resulting from an overall strain deformation of such a core-shell structure, the strain in the front and back end of the particle is assumed to be the same as the overall strain. However, in the middle section, due to the presence of the core, the effective strain within the shell material is higher than the overall strain applied to the whole particle. The corresponding stress response is thus dramatically increased in the middle section, while in the front and back sections we assume the response to be unaffected by the presence of the core. The effective compressive modulus K and shear modulus G of the whole core-shell particle is then estimated by averaging the respective moduli of the three sections weighted by their volume ratios as

$K_{non-linear} = K_{middle-section} \cdot (L_{core}/L) + K_{shell} \cdot (1 - L_{core}/L)$, and Eq. (3).

$G_{non-linear} = G_{middle-section} \cdot (L_{core}/L) + G_{shell} \cdot (1 - L_{core}/L)$, Eq. (4).

where L and L_{core} are the lengths of the cylinders approximating the shapes of the microparticle and its core, and the compressive and shear moduli for the middle section are derived as

$K_{middle-section} = K_{core}(2\varepsilon_{r,core} + \varepsilon_{z,core})/2\varepsilon_r + \varepsilon_z$, Eq. (5).

and

$G_{middle-section} = G_{core}(\varepsilon_{r,core} - \varepsilon_{z,core})/\varepsilon_r - \varepsilon_z$ Eq. (6).

ε_r and $\varepsilon_z$represent the macroscopic strains along the radial and longitudinal directions respectively, while $\varepsilon_{r,core}$ and $\varepsilon_{z,core}$ are radial and longitudinal strains of the core material respectively. (Please see the Supplementary Information for a detailed deduction of the model)

In this simple model, the input moduli of the core and shell material are obtained from independent measurements on single-component microparticles made from the core and shell materials, respectively, using the same technique. In the present case, we measure the shear and compressive moduli of PLGA and alginate of identical composition (Figure S1 (A) and (B)) as in the core-shell particles, and use the measured values, K_{core}=782.25 kPa, K_{shell}=66.89kPa, G_{core}=91.51 kPa, G_{shell}=9.38kPa, as well as the core-to-shell ratios as the input in our simple model for estimating the nonlinear stress response of the core-shell particles. Our simple model thus has no free parameters and predicts the overall response of the core-shell particles based solely on measured quantities. Our simple model predicts that as the core-to-shell ratio α increases, the strain stiffening behavior becomes more pronounced and occurs at smaller strain deformations for both compressive and shear moduli, as shown by the solid lines in Figure 5 (C) and (D).

To validate this simple model, we compare its predictions to measurements of microparticles with different core-to-shell ratios, α= 0.5, α= 0.55 and α= 0.7, respectively. As shown in Figure 5 (E) and (F), despite its simplicity, our model captures the essential behaviors observed experimentally. Even with a small difference in α of 0.05, distinctive behavior is well demonstrated by this simple model (Figure 5 (E) and (F)). The ability to capture distinctive mechanic responses from such a small difference in microstructure is partially due to the fact that the moduli of the core are approximately 10 times larger than that of the shell. Moreover, with the same core-to-shell ratio α=0.55, the particles exhibit similar strain stiffening behavior in both shear and compressive modulus, as shown by the red and blue open symbols in Figure 5 (G). This indicates, besides the moduli of the core and shell materials, the core-to-shell ratio is the most important factor controlling the elastic behavior of the core-shell particles (Figure 5 (C) and (D)).

Our method and simple model description thus provides guidelines for designing core-shell structures with well-defined

nonlinear elastic properties and can serve as a tool to predict their behavior in constricted geometries, such as in small blood vessels.

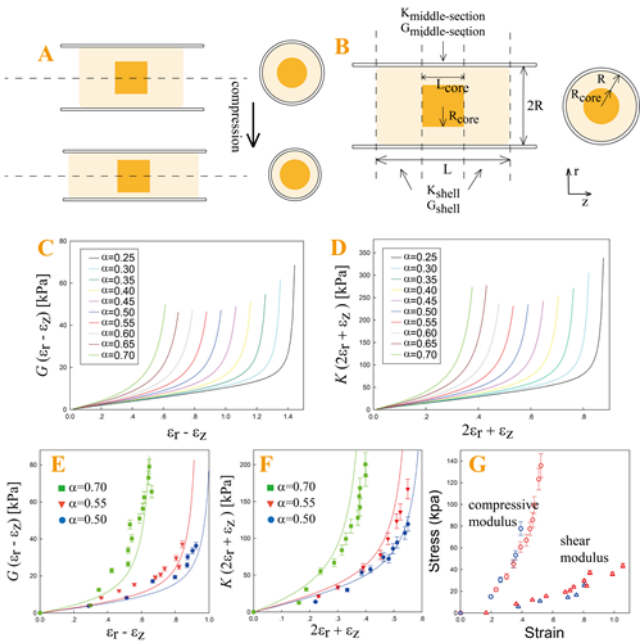

Fig.5 Schematic of the model description: (A) The shape of the core-shell particle is approximated as two cylinders with circular cross section; (B) the core-shell particle is divided into three sections, the section containing the core and the section at the front and back end of the particle. Model predictions of nonlinear elastic response of core-shell particles with different core-to-shell (from α=0.25 to α=0.7) ratios: (C) characteristic shear stress as a function of $\varepsilon_r - \varepsilon_z$; (D) compressive stress as a function of the volumetric strain $2\varepsilon_r + \varepsilon_z$. Experimental data of the nonlinear elastic properties of core-shell particles with different core-to-shell ratios α=0.5 (blue circles), α=0.55 (red triangles), and α=0.7 (green squares); corresponding model predictions are shown as solid lines, in good agreement with the experimental data: (E) Characteristic shear stress as a function of $\varepsilon_r - \varepsilon_z$; (F) Compressive stress as a function of the volumetric strain $2\varepsilon_r + \varepsilon_z$. (G) Stress-strain curves shown for two different particles with the same same α=0.55, illustrating particle-to-particle reproducibility. The error is estimated based on an error propagation analysis[25]; main sources of error include the applied pressure difference and the spatial precision obtained with the digital image analysis.

Conclusions

We have systematically investigated the elastic behavior of composite core-shell microparticles by using Capillary Micromechanics. Our results show that the elastic properties depend sensitively on the core-to-shell ratio and the properties of the core and shell material. In the linear deformation range, the elastic properties of core-shell composite microparticles can be adequately described by the respective moduli of the core and shell weighted by their volume ratios. At deformations beyond the linear elastic regime, we observe a dramatic strain stiffening behavior, which upon increasing the core-to-shell ratio becomes more pronounced and occurs at smaller deformations. We have developed a simple model that captures the essential features of this behavior and enables the design of materials with targeted strain-stiffening behavior in the squeezing mode of deformation that particles undergo when compressed in a capillary. The same mode of deformation is potentially highly relevant in the transport of soft particles in the blood circulation, where the ability of soft particles to squeeze through narrow blood vessels is of key importance.

Acknowledgements

This research was supported by the NWO/RGC Joint Research Scheme sponsored by the Research Grants Council of Hong Kong and the Netherlands Organisation for Scientific Research (D-HK009/11T), the Basic Research Program-General Program (JC201105190878A) from the Science and Technology Innovation Commission of Shenzhen Municipality, the Young Scholar's Program (NSFC51206138/E0605) from the National Natural Science Foundation of China as well as the Seed Funding Program for Basic Research (201101159009), Small Project Funding (201109176165) from the University of Hong Kong, and the Research Grants Council of Hong Kong (GRF718111 and GRF717613). This research was also supported in part by the Zhejiang Provincial, Hangzhou Municipal and Lin'an County Governments.

Notes and references

[a]*Department of Mechanical Engineering, The University of Hong Kong, Pokfulam Road, Hong Kong; E-mail: ashum@hku.hk;lqwang@hku.hk*
[b]*HKU- Zhejiang Institute of Research and Innovation (HKU-ZIRI), 311100, Hangzhou, Zhejiang, China*
[c]*Eindhoven University of Technology, ICMS & Department of Mechanical Engineering, 5600 MB Eindhoven, The Netherlands; E-mail: H.M.Wyss@tue.nl*
[d]*HKU-Shenzhen Institute of Research and Innovation (HKU-SIRI), 518000, Shenzhen, Guangdong, China*

† Electronic Supplementary Information (ESI) available: [Details of fabrication of Capillary Micromechanics device and mechanism of Capillary Mircomechanics. Characterization of mechanical properties of single PLGA and alginate microparticles. Detailed deduction of model to describe the strain stiffening behavior of core-shell microparticles with different α.]. See DOI: 10.1039/b000000x/

1. A. Abbaspourrad, N. J. Carroll, S.-H. Kim, and D. A. Weitz, *J. Am. Chem. Soc.*, 2013, 7744−775.
2. W. J. Duncanson, T. Lin, A. R. Abate, S. Seiffert, R. K. Shah, and D. A. Weitz, *Lab Chip*, 2012, **12**, 2135–45.
3. J.-W. Kim, A. S. Utada, A. Fernández-Nieves, Z. Hu, and D. a Weitz, *Angew. Chem. Int. Ed. Engl.*, 2007, **46**, 1819–22.
4. S. Seiffert, *Macromol. Rapid Commun.*, 2011, **32**, 1600–9.
5. T. S. Shim, S.-H. Kim, and S.-M. Yang, *Part. Part. Syst. Charact.*, 2013, **30**, 9–45.
6. G. Sukhorukov, A. Fery, and H. Möhwald, *Prog. Polym. Sci.*, 2005, **30**, 885–897.
7. M. Malmsten, *Soft Matter*, 2006, **2**, 760.
8. E. Pisani, N. Tsapis, J. Paris, V. Nicolas, L. Cattel, and E. Fattal, *Langmuir*, 2006, **22**, 4397–402.

9. R. Díaz-López, N. Tsapis, D. Libong, P. Chaminade, C. Connan, M. M. Chehimi, R. Berti, N. Taulier, W. Urbach, V. Nicolas, and E. Fattal, *Biomaterials*, 2009, **30**, 1462–72.

10. Y. Zhao, X. Zhao, B. Tang, W. Xu, J. Li, J. Hu, and Z. Gu, *Adv. Funct. Mater.*, 2010, **20**, 976–982.

11. S. Gouin, *Trends Food Sci. Technol.*, 2004, **15**, 330–347.

12. S. Seiffert and J. Thiele, *J. Am. …*, 2010, **01238**, 6606–6609.

13. G. B. Sukhorukov, A. L. Rogach, M. Garstka, S. Springer, W. J. Parak, A. Muñoz-Javier, O. Kreft, A. G. Skirtach, A. S. Susha, Y. Ramaye, R. Palankar, and M. Winterhalter, *Small*, 2007, **3**, 944–55.

14. M. H. Lee, K. C. Hribar, T. Brugarolas, N. P. Kamat, J. A. Burdick, and D. Lee, *Adv. Funct. Mater.*, 2012, **22**.

15. O. I. Vinogradova, O. V. Lebedeva, and B.-S. Kim, *Annu. Rev. Mater. Res.*, 2006, **36**, 143–178.

16. S. She, C. Xu, X. Yin, W. Tong, and C. Gao, *Langmuir*, 2012, **28**, 5010–6.

17. S. S. Datta, S.-H. Kim, J. Paulose, A. Abbaspourrad, D. R. Nelson, and D. a. Weitz, *Phys. Rev. Lett.*, 2012, **109**, 134302.

18. S. S. Datta, H. C. Shum, and D. a Weitz, *Langmuir*, 2010, **26**, 18612–6.

19. T. Still, R. Sainidou, M. Retsch, and U. Jonas, *Nano Lett.*, 2008.

20. T. S. Shim, S.-H. Kim, C.-J. Heo, H. C. Jeon, and S.-M. Yang, *Angew. Chem. Int. Ed. Engl.*, 2012, **51**, 1420–3.

21. S. Leick, M. Kott, P. Degen, S. Henning, T. Päsler, D. Suter, and H. Rehage, *Phys. Chem. Chem. Phys.*, 2011, **13**, 2765–73.

22. S. Leick, A. Kemper, and H. Rehage, *Soft Matter*, 2011, **7**, 6684.

23. G. Sun and Z. Zhang, *Int. J. Pharm.*, 2002, **242**, 307–11.

24. Y. Zhao, H. C. Shum, L. L. A. Adams, B. Sun, C. Holtze, Z. Gu, and D. A. Weitz, *Langmuir*, 2011, 13988–13991.

25. H. M. Wyss, T. Franke, E. Mele, and D. A. Weitz, *Soft Matter*, 2010, **6**, 4550.

26. M. Guo and H. M. Wyss, *Macromol. Mater. Eng.*, 2011, **296**, 223–229.

27. K. Hidaka, L. Moine, G. Collin, D. Labarre, J. L. Grossiord, N. Huang, K. Osuga, S. Wada, and A. Laurent, *J. Mech. Behav. Biomed. Mater.*, 2011, **4**, 2161–7.

28. R. Skalak and P. I. Branemark, *Science*, 1969, **164**, 717–9.

29. J. P. Best, Y. Yan, and F. Caruso, *Adv. Healthc. Mater.*, 2012, **1**, 35–47.

30. A. Banerjee, M. Arha, S. Choudhary, R. S. Ashton, S. R. Bhatia, D. V Schaffer, and R. S. Kane, *Biomaterials*, 2009, **30**, 4695–9.

31. L. Brannon-Peppas, *Int. J. Pharm.*, 1995, **116**, 1–9.

32. D. Kohane, *Biotechnol. Bioeng.*, 2007, **96**, 203–209.

33. E. Tomlinson, *J. Control. Release*, 1985, **2**, 385–391.

34. J. J. Liétor-Santos, B. Sierra-Martín, and A. Fernández-Nieves, *Phys. Rev. E*, 2011, **84**, 060402(R).

35. A. R. Abate, L. Han, L. Jin, Z. Suo, and D. a. Weitz, *Soft Matter*, 2012.

36. B. Sierra-Martin, J. A. Frederick, Y. Laporte, G. Markou, J. J. Lietor-Santos, and A. Fernandez-Nieves, *Colloid Polym. Sci.*, 2010, **289**, 721–728.

37. E. A-Hassan, W. F. Heinz, M. D. Antonik, N. P. D'Costa, S. Nageswaran, C. a Schoenenberger, and J. H. Hoh, *Biophys. J.*, 1998, **74**, 1564–78.

38. S. C. W. Tan, W. X. Pan, G. Ma, N. Cai, K. W. Leong, and K. Liao, *BMC Cell Biol.*, 2008, **9**, 40.

39. R. Kwok and E. Evans, *Biophys. J.*, 1981, **35**, 637–52.

40. O. Tagit, N. Tomczak, and G. J. Vancso, *Small*, 2008, **4**, 119–26.

41. N. P. Kamat, M. H. Lee, D. Lee, and D. A. Hammer, *Soft Matter*, 2011, **7**, 9863–9866.

42. P. Preira, V. Grandné, J.-M. Forel, S. Gabriele, M. Camara, and O. Theodoly, *Lab Chip*, 2013, **13**, 161–70.

43. J. Liu, Y. Yap, and N.-T. Nguyen, *Phys. Rev. E*, 2009, **80**, 046319.

44. J. Liu, Y. F. Yap, and N.-T. Nguyen, *Microfluid. Nanofluidics*, 2008, **6**, 835–846.

45. H. Lan and D. B. Khismatullin, *Int. J. Multiph. Flow*, 2012, **47**, 73–84.

46. H. Bow, I. Pivkin, M. Diez-Silva, and S. Goldfless, *Lab Chip*, 2011, **11**, 1065–1073.

47. H. M. Wyss, J. M. Henderson, F. J. Byfield, L. A. Bruggeman, Y. Ding, C. Huang, J. H. Suh, T. Franke, E. Mele, M. R. Pollak, J. H. Miner, P. A. Janmey, D. A. Weitz, and R. T. Miller, *Am J Physiol Cell Physiol*, 2011, **300**, 397–405.

48. T. Tominaga, N. Takedomi, H. Biederman, H. Furukawa, Y. Osada, and J. P. Gong, *Soft Matter*, 2008, **4**, 1033.